Thermal effects in the x-ray spectra of $La_{1-x}Ca_xMnO_3$

Q. Qian,[1] T. A. Tyson,[1] C.-C. Kao,[2] M. Croft,[3] S.-W. Cheong,[3] and M. Greenblatt[4]
[1]*Department of Physics, New Jersey Institute of Technology, Newark, New Jersey 07102*
[2]*Brookhaven National Laboratory, Upton, Long Island, New York 11973*
[3]*Department of Physics and Astronomy, Rutgers University, Piscataway, New Jersey 08854*
[4]*Department of Chemistry, Rutgers University, Piscataway, New Jersey 08854*
(Received 3 January 2000)

Complementary x-ray emission (XES) and x-ray-absorption (XAS) measurements of $La_{1-x}Ca_xMnO_3$ as a function of temperature have been performed. For $0.5 \leqslant x \leqslant 0.8$ we find changes in the XAS and XES spectra consistent with a small increase in the average Mn valence accompanying the passage to the low-temperature state. It is suggested that this small Mn-configuration shift could be due to the competition between the energies associated with ferromagnetic (FM) and charge/orbital (CO) correlations. In the region $0.0 \leqslant x \leqslant 0.4$ we observe thermal spectral changes quite different from those found in the $x \geqslant 0.5$ materials. Modest thermal changes in the Mn XAS pre-edge (*K*-edge), for $0.0 \leqslant x \leqslant 0.4$, were observed to be coupled to the robustness of the FM-metallic ground state. The clearest pre-edge feature variation appears to be related to Mn-e_g-majority-spin state changes. In contrast the thermal XES spectral changes appear similar in character in the antiferromagnetic (AF)-insulating $x=0.0$ and FM-metallic $x=0.3$ materials. An enhancement of the effective local moment via a coupling to the internal exchange field, in the magnetically ordered states, is proposed to explain these XES results. The $x=1.0$ end member ($CaMnO_3$) was found to exhibit significant temperature dependence of the absorption and emission spectra. These XAS and XES results, for $CaMnO_3$, are discussed in terms of thermal perturbations on the degree of covalency of this material.

I. INTRODUCTION

There is much conflicting data on the valence/*d*-configuration of Mn as a function of doping and temperature in the manganite system $La_{1-x}Ca_xMnO_3$. In thermoelectric power experiments (TEP), Hundley and Neumeier[1] found that more holelike charge carriers or alternatively fewer accessible Mn sites are present than expected for the value *x*. They suggest a charge disproportionation model based on the instability of Mn^{3+}-Mn^{3+} relative to that of a Mn^{2+}-Mn^{4+}. Using electron paramagnetic resonance (EPR) measurements Oseroff *et al.*[2] suggest that below 600 K there are no isolated Mn atoms of valency +2, +3, or +4. However, they argue that EPR signals are consistent with a complex magnetic entity composed of Mn^{3+} and Mn^{4+} ions. Based on Mn $2p$ x-ray photoemission (XPES) and O $1s$ absorption, Park *et al.*[3] support the double exchange theory with separate site valence mixing of Mn^{3+}/Mn^{4+} ion. They were able to obtain approximate spectra of the intermediate doping XPES spectra by linearly combining the end-member spectra, consistent with a linear change of spectral features with doping. However, the significant discrepancy between the weighted spectrum and the prepared spectrum (for given *x*) suggests a more complex doping effect. Subias *et al.*[4] examined the valence state of Mn utilizing Mn *K*-edge absorption measurements and found a large discrepancy between intermediate doping spectra and linear combinations of the end members. They suggest that Mn did not fluctuate between ioniclike 3+ and 4+. From Mn x-ray magnetic dichroism measurements, they argue that Mn exists in a unique magnetic state. Systematic shifts in the absorption edge position with doping have been found by Subias *et al.* (Mn *K*-edge),[4] Booth *et al.* (Mn *K*-edge),[5] Croft *et al.* (Mn *K*-edge),[6] Liu *et al.* (Mn *L*-edge), and Pellegrin *et al.* (Mn *L*-edge and O *K*-edge).[7] Recently, Bridges *et al.*[8] reported that changes in the weak pre-edge (Mn *K*-edge) exhibit temperature dependence only for colossal magnetoresistance (CMR) (metallic) samples. The nature of the valence of Mn and, in general, the electronic structure in these systems are central to determining the essential physics of these materials. Moreover, any temperature-dependent changes in valence may shed light on the physics of the insulator-to-metal transitions.

The Mn K_β emission spectrum provides a direct method to probe the total Mn $3d$ spin *S* and effective charge density on the Mn sites as has been shown in our previous work on the manganites.[9] The main line position depends on the oxidation, covalency, and spin state of the transition-metal ion. The details of the multiplet structure depend on the spin alignment (high spin vs. low spin). The point group symmetry of the Mn site (crystal field effects) impact the spectra to a lesser extent.[10–12] XAS spectra (as will be seen in detail below) are determined by both the local structural arrangement about the Mn site and by the valence of Mn site. The combined measurements can be used to elucidate the question of valence/*d* configuration in the manganite system.

In order to understand the trends in the Mn valence/*d*-configuration as a function of temperature in distinctly different doping regimes of the manganites, we have performed complementary Mn K_β edge measurements of the $La_{1-x}Ca_xMnO_3$ manganite system. The disparate thermal spectral changes observed motivate discussion of the results in three separate regions/cases: $0.5 \leqslant x \leqslant 0.8$, $0.0 \leqslant x \leqslant 0.4$, and $x=1.0$. In an attempt to understand these modest, but clearly discernable, spectral changes, the intrinsic covalent-*d*-configuration admixture of the Mn will be invoked along with a competition between ferromagnetic-correlations,

charge/orbital-correlations and thermal energy scales. Below some of the principal results in the different composition ranges are noted and a summary of the organization of the paper is presented.

For $0.5 \leqslant x \leqslant 0.8$ we find changes in both the XAS and XES spectra empirically consistent with a small increase in the average Mn valence accompanying the transition to the low-temperature state. In the region $0.0 \leqslant x \leqslant 0.4$ we observe trends fundamentally different from those found in the $0.5 \leqslant x \leqslant 0.8$ materials. Interestingly, in the $x \leqslant 0.4$ materials the XES and XAS results do not at present appear mutually amenable to a simple thermal valence variation explanation. The XES results appear consistent with a small enhancement of the local magnetic spin moment accompanying the onset of static magnetic order. Importantly, this local spin enhancement is common to both the $x=0.0$ antiferromagnetic insulator (AF-*I*) and $x=0.3$ ferromagnetic metal-(FM-*M*). In contrast, the small thermal changes in the XAS pre-edge (in the $x \leqslant 0.4$ regime) appear to scale with the FM-*M* energy, namely the XAS pre-edge effect is maximal near $x=0.3$ and appears nearly absent near $x=0.0$. The thermal pre-edge XAS variation in the FM-*M* regime appears to principally involve modification of the majority-spin e_g states. Finally, thermal XES and XAS results on the end member $x=1.0$ ($CaMnO_3$) although modest, are seen to be larger than expected.

Since this paper involves complementary XES and XAS studies on the $La_{1-x}Ca_xMnO_3$ system, which manifests multiple regimes with distinct physical behavior, we will briefly review the organization of the paper. After this introduction the experimental details will be discussed in Sec. II. Since the clearest correlations between our XES and XAS results appear in the $0.5 \leqslant x \leqslant 0.8$ range, this regime will be discussed first in Sec. III. The background of Mn compound XES is briefly reviewed in Sec. III A and the temperature-dependent XES results (for $x=0.5$) are discussed in Sec. III B. The signatures of Mn-valence variations in the XAS is reviewed in Sec. III C and the temperature-dependent XAS results, for $0.5 \leqslant x \leqslant 0.8$ compounds, are discussed in Sec. III D. A mechanism, based on the competition between high-temperature FM correlations and low-temperature CO correlation, is proposed in Sec. III E to explain both the XES and XAS results for $0.5 \leqslant x \leqslant 0.8$. Section IV will address the $0.0 \leqslant x \leqslant 0.4$ range of compounds. Comparison of the temperature-dependent XES results for the AF-*I* $x=0.0$ and FM-*M* $x=0.3$ compounds is made in Sec. IV A. The similarity of this comparison motivates the introduction, in Sec. IV B, of a mechanism (based on a modest interatomic exchange enhancement of the Mn moment) to explain the thermal XES variation in this range. The thermal variation of the XAS results in the $0.0 \leqslant x \leqslant 0.4$ range are then discussed in Sec. IV C and contact is made with the results of Bridges *et al.*[8] for this same range. The robust thermal variation of the XES and XAS of $CaMnO_3$ are then discussed in Sec. V. Finally, the results are summarized in Sec. VI.

II. EXPERIMENTAL METHODS

Samples of $La_{1-x}Ca_xMnO_3$ were synthesized (in air) and characterized as described by the standard solid-state method.[6] Fluorescence measurement samples were prepared by finely grinding the materials and packing them onto adhesive tape.

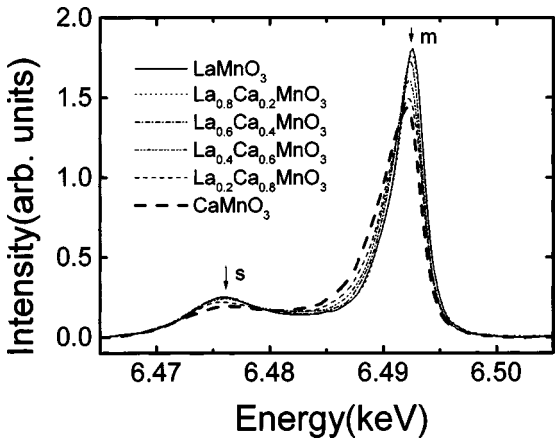

FIG. 1. Mn K_β spectra of $La_{1-x}Ca_xMnO_3$ with Ca doping: $x=0$, 0.2, 0.4, 0.6, 0.8, 1. The spectra display a clear change of shape [main line (*m*) position and width as well as satellite (*s*) width] with doping level. Note that all spectra are area normalized over the region given.

The Mn K_β fluorescence measurements were performed at the National Synchrotron Light Source's (NSLS) 27 pole wiggler Beamline X21A. The experimental setup, which consists of an analyzer and detector in Rowland geometry, is described in Ref. 13 and previously published data on the manganite system can be found in Ref. 9.

An incident energy ($\hbar\omega$) of 6556 eV was selected using a four-bounce Si (220) monochromator. The incident energy was calibrated by the known Mn metal *K*-edge absorption inflection point (6539 eV). Five spherically bent Si (220) analyzer crystals were used to resolve the energy of the emitted photons, $\hbar\Omega$. A solid-state Bicron NaI scintillation counter was used to measure the fluorescence radiation. The absolute fluorescence photon energy was calibrated from the elastic scattering peaks of the sample at the same position utilizing the known incident energy. Due to the attenuation of the beam by the Be windows of the cryostat, 2–3 scans were required for temperature-dependent measurements. Error bars were determined by assuming a Gaussian distribution in the number of counts at each energy point. The x-ray-absorption spectra were measured at beamline X11A, X18B, and X19A using Si (111) monochromators. Normalization of the data followed standard procedures.[14] For temperature-dependent measurements, Displex™ based cryostats or pour fill liquid-nitrogen cryostats with sensors near the sample positions were used.

III. $La_{1-x}Ca_xMnO_3$: $0.5 \leqslant x \leqslant 0.8$ REGIME; CO GROUND-STATE/HT-FM-CORRELATIONS COMPETITION

A. Mn-compound XES

The Mn K_β emission entails the $3p \rightarrow 1s$ x-ray transition decay process that follows the core $1s$ hole created in Mn *K*-edge x-ray absorption. Referring to Fig. 1, the central structure in the Mn K_β spectrum is a sharp, intense main (*m*) line (~6492 eV) and a broad, low intensity satellite (*s*) line at lower energy (~6476 eV). The *m* line (*s* line) is primarily

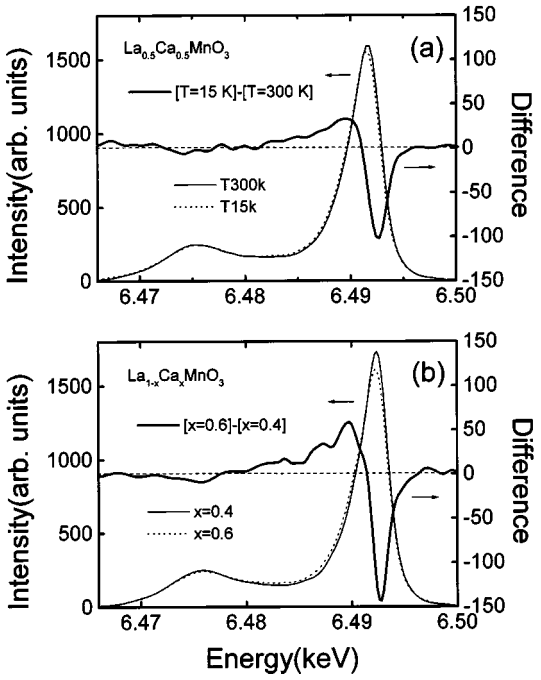

FIG. 2. (a) A comparison of the $T=300$ K and $T=15$ K Mn K_β emission spectra of $La_{1-x}Ca_xMnO_3$, $x=0.5$. The difference of these two spectra is also shown with the scale for the difference spectrum (DS) appearing on the right; (b) A comparison of the room-temperature $x=0.4$ and 0.6 and $T=15$ K Mn K_β emission spectra of the $La_{1-x}Ca_xMnO_3$ system. The difference of these two spectra is also shown with the scale for the difference spectrum (DS) appearing on the right. Note the similarities of the change in spectrum with doping and the temperature dependent changes in the $x=0.5$ sample.

due to $3p \rightarrow 1s$ decay process in which the now unpaired $3p$ electron spin is aligned (antialigned) with the $3d$ orbital spin. Qualitatively, the energy splitting between the main line and satellite is given by $\Delta E_{sm}=J(2S+1)$ while the intensity ratio of the satellite to the main peak is given by $I_s/I_m=S/(S+1)$, where S is the total spin of the unpaired electrons in the $3d$ shell and J is the exchange integral.[15] Solid-state covalency or $3d$-itineracy effects reduce the atomic exchange effects in these emission spectra. Specifically, the ΔE_{sm} value is reduced and the s line broadened and weakened by such solid-state effects (see Ref. 9). The details of the emission spectral changes with the Mn spin and charge state involve multiple satellite contributions in addition to the m and s lines. Nevertheless, recent work on Mn-oxide materials has demonstrated systematic changes with Mn valence (see Ref. 9 and references therein). In Fig. 1, for example, the Mn-valence increase is seen to be reflected in the m-line shift to lower energy and strong broadening on its low-energy side, and the intensity loss/broadening of the s line.

B. T-dependent XES results for $x=0.5$

Comparison of the $T=300$ K and $T=15$ K emission spectra for the $x=0.5$ material, in Fig. 2(a), reveals small but clearly perceptible thermal changes. This change is emphasized by the difference spectrum (DS) also shown in Fig. 2(a). Referring back to Fig. 1 one notes that increasing x induces spectral changes similar to (albeit much larger than) the thermal changes observed in Fig. 2(a). To better test this notion the $x=0.4$ and $x=0.6$ spectra, and their difference spectrum (corresponding to a formal Mn-valence change of 0.2) are shown in Fig. 2(b). The difference spectra in Figs. 2(a) and 2(b) are quite similar in structure with the magnitude of the $x=0.5$ thermal difference spectra being smaller. Specifically, the proportional magnitude of the $x=0.5$ thermal DS is more consistent with an average Mn-valence increase closer to 0.1 on cooling from 300 to 15 K.

This interpretation of a valence increase at lower temperatures in the $x=0.5$ materials is, of course, entirely empirical. If, however, the thermal spectral changes are caused by other effects, within the XES data at hand, such effects must conspire to resemble those of a small valence change. Thus the valence change interpretation has both the merits of accurate description and simplicity.

In the past, Mn K near-edge XAS has proved useful in identifying the robust changes in Mn valence with composition in this $La_{1-x}Ca_xMnO_3$ system.[6] However, XAS has not heretofore been able to identify such subtle thermal Mn-valence changes as suggested above by the XES results. The temperature dependence of the near-edge XAS, for the $x=0.5$ material, will be re-examined, below, with this in mind.

C. Mn-compound XAS

The Mn K-edge spectra of the formally Mn^{3+}-$LaMnO_3$ and Mn^{4+}-$CaMnO_3$ are shown in Fig. 3. These standard spectra facilitate the itemization of three distinct spectral signatures previously used to identify a Mn-valence increase.[6] First, the main edge B feature (due to transitions into $4p$ states) exhibits a large chemical shift to higher energy in the Mn^{3+} to Mn^{4+} change. This shift has been shown to scale with the average Mn valence.[6]

Second, the pre-edge a feature changes both in spectral structure and intensity.[16] The $CaMnO_3$ pre-edge exhibits three sub features (see Fig. 3, left inset), a strong peak $a2$, a weaker shoulder $a1$, and a subtle third peak $a3$ which is typically only discernable in high-resolution and high signal-to-noise data.[17] In the $LaMnO_3$ pre-edge the two unresolved $a1$ and $a2$ subfeatures have comparable intensities (see Fig. 3, left inset) and are clearly shifted to lower energies relative to the $a1$ and $a2$ features in $CaMnO_3$. In the $La_{1-x}Ca_xMnO_3$ system, the pre-edge structure evolves with increasing x between these two limiting structures.

Third, in the main portion of Fig. 3, the prominent D feature (15–20 eV above the B peak) should be noted in the Mn^{4+}-$CaMnO_3$ spectrum. This D feature has been observed to appear and grow systematically with increasing Mn^{4+} content in such perovskite related materials.[16]

D. Temperature-dependent XAS $x=0.5$, 0.67, 0.8

The detailed variation of the $x=0.5$ spectrum (see Fig. 3 and insets) between $T=300$ K and $T=15$ K will now be considered with respect to each of these three signatures. First, the main B-feature peak (see Fig. 3 bottom inset) can be seen to exhibit a small but discernable shift to higher energy upon

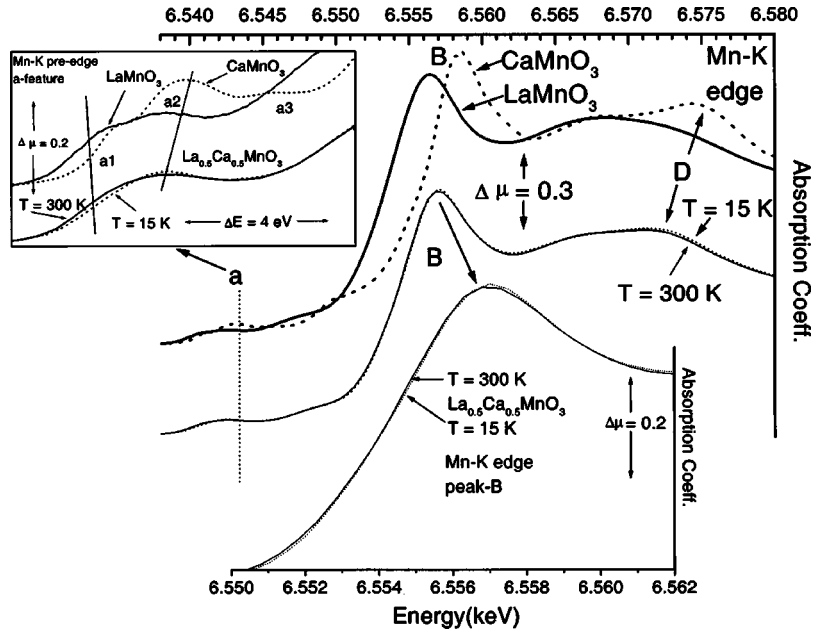

FIG. 3. The Mn *K*-edge of $CaMnO_3$, $LaMnO_3$, and $La_{0.5}Ca_{0.5}MnO_3$ at $T=300$ and 15 K. The upper left inset shows an expansion of the pre-edge *a*-feature region (note peaks $a1$, $a2$, and $a3$) and the lower right inset shows an expansion of the main peak (*B*).

cooling from 300 to 15 K. This shift would be consistent with a small increase in the average Mn valence accompanying this temperature decrease. (It should be noted that only by the simultaneous standard method and with high quality standard data could this small shift be detected. Further multiple independent measurements were undertaken to verify this and other subtle spectral changes discussed in this paper.)

Second, upon cooling from 300 to 15 K the pre-edge feature (see Fig. 3, left inset) of the $x=0.5$ material manifests a small but quite distinct intensity loss on the low-energy side of the $a1$ feature (the position being highlighted by a line in the inset); and a smaller, but still visible, intensity enhancement of the high-energy side of the $a2$ feature (highlighted by a line in the inset). Again, the two most prominent pre-edge spectral changes are those expected to accompany an increase in the Mn valence on cooling the $x=0.5$ material from 300 to 15 K.

Third, the reader is referred to the *D*-feature region 15–20 eV above the *B*-feature peak (Fig. 3). There is a small but discernable enhancement of the spectral intensity of the $T=15$ K spectrum, relative to the $T=300$ K spectrum, in this *D*-feature range (highlighted with an arrow in the Fig. 3). Here again this subtle change is in precisely the right place to reflect a small Mn-valence change (increase) in the $x=0.5$ material upon cooling from 300 to 15 K.

Thus all three of the near-edge XAS signatures support an increase in the average Mn valence (albeit quite small) on cooling the $x=0.5$ from 300 to 15 K. Taken with the same indication in the temperature-dependent XES results they cumulatively add credence to this interpretation.

For later consideration, note in Fig. 4 the thermal variation of the pre-edges of the $x=0.5$, $x=0.67$, $x=0.8$, and $x=1.0$ materials. The $x=0.67$ material manifests a thermal change similar to, but smaller than, that of the $x=0.5$ material. This thermal effect is smaller yet for the $x=0.8$ material. The same quenching of the temperature dependence

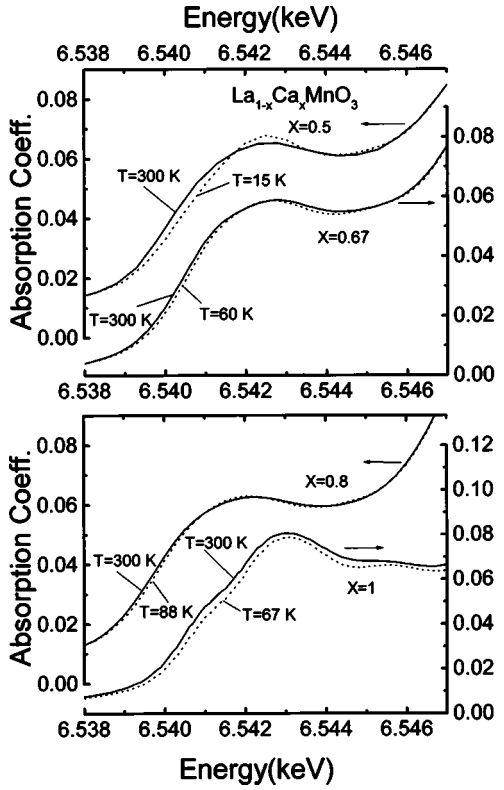

FIG. 4. The Mn pre-edge feature (*K*-edge, *a*-feature region) of $La_{1-x}Ca_xMnO_3$ with $x=0.5$, 0.67, 0.8, and 1.0 at different temperatures. Note the very small change with temperature observed in the $x=0.8$ system.

near $x=0.8$ has also been found by in the insulating $Bi_{1-x}Ca_xMnO_3$ system.[18]

E. Mechanism: $0.5 \leqslant x \leqslant 0.8$ regime

The evidence from the XES and XAS results are mutually consistent with a slight increase in the average Mn valence at lower temperatures in the $x=0.5$ (and from Fig. 4 apparently also in the $x=0.67$) material. This motivates consideration of a common potential origin for these effects. In what follows, an argument is presented that proposes the energy of the FM interactions at 300 K in these materials stabilizes lower average Mn valence (a greater Mn^{3+} admixture); invokes the known suppression of FM correlations in the low-temperature CO ordered phase and finally proposes the relaxation of the Mn valence to a higher value when FM correlations (supporting the excess Mn^{3+} content) are quenched in the CO ordered phase.

The low-temperature state, in this composition range, for these substituted manganites, is a ''charge/orbital ordered'' one in which hole hopping is condensed out. The room-temperature phase, on the other hand, supports strong FM correlation. Specifically, the ferromagnetism in these manganites originates from the double exchange interaction between a Mn^{3+} and Mn^{4+} bridged by a covalently bonded O atom. The additional caveat on this FM interaction is that static charge order is absent so that the Mn^3+/Mn^{4+} sites are free to resonantly interchange. Magnetic and neutron-scattering studies clearly demonstrate that FM correlations are present in such highly doped materials ($x \geqslant 0.5$) at high temperatures, and that the FM correlations are suppressed upon the onset of charge ordering at lower temperatures.[19]

Empirically the phase diagrams indicate that the FM ordering temperature (and energy) reaches its maximum value (250–350 K) in these $La_{1-x}A_xMnO_3$ materials in the $x=0.3-0.4$ range. On general theoretical grounds, such double exchange would reach its maximum at $x=0.0$ and $x=0.5$ for the limits of zero and infinite correlations in the Mn-e_g band, respectively.[20] Thus on both experimental and theoretical grounds the optimization of the FM interaction at a value less than $x=0.5$ (i.e., less than 50% Mn^{3+}/Mn^{4+} admixture) is expected. Specifically, for a material with $x \geqslant 0.5$, the FM-interaction–energy should favor the alteration of available electronic degrees of freedom toward those values at which it is maximal (i.e., similar to those with x in the 0.3–0.4 range).

Although many phenomena in these manganites are qualitatively discussed in terms of ionic mixtures of $Mn^{3+}(d^4)$ and $Mn^{4+}(d^3)$, there are substantial covalency effects in these systems.[9] From the view point of the Mn-d configurations this means that the Mn sites actually involve a mixture of $Mn^{3+}(d^4)$ and $Mn^{4+}(d^3)$, configurations. The hopping charge carriers involve O-p as well as Mn-e_g content. The notion of charge hopping will therefore involve Mn-site configurations which are bimodal (in the presence or absence of a hole), however, they are covalent configurational admixtures in both states. Thus changes in the balance of the energy parameters (e.g., the Jahn-Teller, FM, or CO effects) at a fixed composition x can alter the balance of the Mn configurations and thereby alter (in a second-order way) the effective average Mn valence of the system. The Mn configurations (in both the hole/no-hole states) must therefore be considered as polarizable (with respect to the average d occupancy) and capable of responding to these competing energies.

Applying these ideas to the case at hand, at 300 K (for the $x=0.5$ material) the FM interaction energy should pull the average Mn valence toward a value where the FM interactions are maximal (i.e., toward a value closer to that when x was closer to 0.3). The destruction of the FM interactions with the low-temperature onset of the CO ordered state, should also quench this valence-pulling and the average Mn valence should increase slightly in the charge ordered state.

In the $x=0.67$ material the FM interactions are still present at room temperature, however, (compared to the $x=0.5$ material) the departure of the system from the ''optimal'' FM configuration is larger. Moreover, the charge ordering temperature (energy scale) is higher in the $x=0.67$ material, hence CO correlations should further reduce the FM effects at room temperature. These effects should combine to yield a reduction of the thermal pre-edge XAS change in the $x=0.67$ spectrum, as seen in results in Fig. 4. Finally, at $x=0.8$ both the competing FM interaction and long-range CO ordering interaction effects are dying off due to the small Mn^{3+}/Mn^{4+} ratio. Thus the observed virtual disappearance of the thermal pre-edge variation effect (see Fig. 4) in this $x=0.8$ material is also understandable.

IV. $La_{1-x}Ca_xMnO_3$: $0.0 \leqslant x \leqslant 0.4$ REGIME; AF-*I*/FM-*M* CROSSOVER

A. *T*-dependent XES results for $x=0.0$ and $x=0.3$

The Mn K_β emission spectra, at $T=300$ K and $T=15$ K, are shown in Fig. 5(a) for $La_{0.7}Ca_{0.3}MnO_3$ and in Fig. 5(b) for $LaMnO_3$. Following the analysis above, the difference spectra formed by subtracting the spectra at the two temperatures are also shown. Comparing the thermal DS for the $x=0.5$ material in Fig. 2(a) to that of the $x=0.3$ material in Fig. 5(a) one notes a striking difference. In the vicinity of the main line the signs of the DS are reversed. Moreover, for the $x=0.3$ material there is a substantial positive region in the DS in the vicinity of the satellite line corresponding to a spectral enhancement in the 15 K spectrum. The presence of quite similar (but somewhat smaller magnitude) thermal effects in the emission spectra [Fig. 5(b)] of the AF material $LaMnO_3$ is particularly significant. Together, these results appear to rule out a mechanism based (for the XES results) purely on the FM ordering and concomitant metallization of the $x \sim 0.3$ material.

Noting that the sign of the thermal DS for the $x=0.0$ and $x=0.3$ materials (Fig. 5) is opposite to that of the thermal DS for the $x=0.5$ material [Fig. 2(a)] raises the possibility of a low-temperature decrease in the Mn valence in the former. Accordingly, in Fig. 5(c), difference spectra formed by subtracting the emission spectra at differing x values, in the low doping range, were compared to those in Figs. 5(a) and 5(b). These comparisons were unsatisfactory in detail in gross structure in the satellite line region. Thus interpretation of the thermal emission spectrum variation (in these low doping materials) solely in terms of a small Mn-valence change ap-

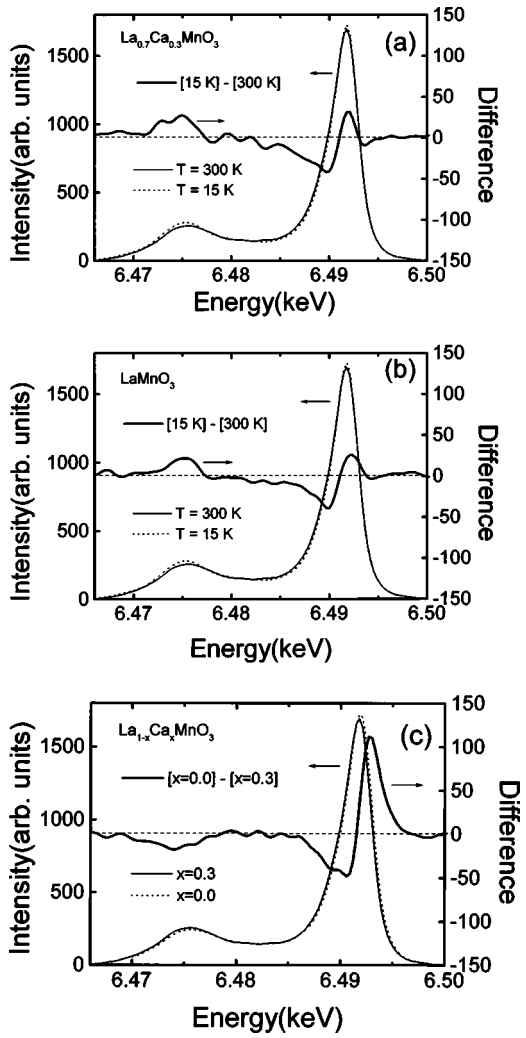

FIG. 5. (a) A comparison of the $T=300$ K and $T=15$ K Mn K_β emission spectra of $La_{1-x}Ca_xMnO_3$, $x=0.3$. The difference of these two spectra is also shown with the scale for the difference spectrum (DS) appearing on the right; (b) A comparison of the $T=300$ K and $T=15$ K Mn K_β emission spectra of $LaMnO_3$. The difference of these two spectra is also shown with the scale for the difference spectrum (DS) appearing on the right. The same temperature trend is observed in both systems. (c) The corresponding comparison of the room-temperature $x=0.0$ and 0.3 Mn K_β emission spectra including the DS.

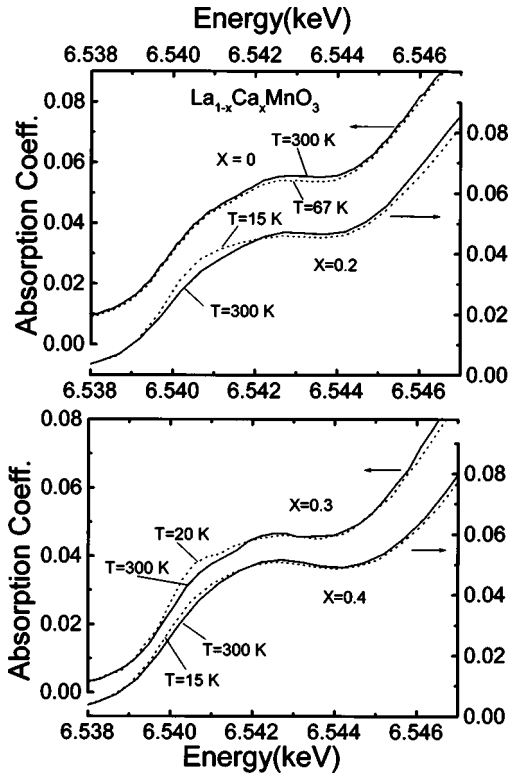

FIG. 6. The pre-edge XAS (Mn K) feature of $La_{1-x}Ca_xMnO_3$ with $x=0.0$, 0.2, 0.3, 0.4 at different temperatures. Note that the temperature dependence is reversed to that found for $x\geqslant 0.5$ in Fig. 4.

pears to be unsatisfactory. This is a nontrivial observation since it stands in contrast to the $x=0.5$ (or higher) material discussion above.

B. XES mechanism for $x=0.0$ and $x=0.3$

Closer inspection of the DS in Fig. 5(a) and 5(b) reveals that one of their salient features is the shifting of spectral intensity at the main line to higher energy and at the satellite line toward lower energy. Thus there is an effective increase in the overall splitting of the main and satellite lines at lower temperature. Recall this overall splitting $\Delta E_{sm}\propto J(2S+1)$, where S is the effective $3d$ atomiclike spin and J is the FM intra-atomic exchange interaction. The $3d$ spin S can be reduced from the atomic value through interatomic covalency or itinerancy effects. (For the purpose of this discussion the covalency/itinerancy renormalization will be assumed to subsumable into the effective local spin value S. More subtle discussion of the partial exchange constant contribution to this reduction will be deferred.) Indeed, theoretical modeling of the XES in Mn-O materials explicitly requires the inclusion of such a covalency reduction factor.[9]

Coherent interatomic magnetic interactions, in a magnetically ordered state, can act to partially undue the covalency reduction in S. Essentially this is a moment enhancement (or a diminution in the moment reduction) in response to the internal exchange field and should scale with the magnitude of the static magnetization (or sublattice magnetization). The effective increase in ΔE_{sm} (evidenced by the data in Fig. 4) is consistent with a partial quenching of the covalency reduction or a local spin enhancement in response to the spontaneous magnetization in the ordered states. In the case of the $x=0.3$ material the response of S is to the spontaneous FM exchange field. In the case of the $x=0.0$ material the response of S is to the spontaneous AF staggered internal field. The somewhat smaller effect in the $x=0.0$ AF material can be ascribed to the fact that it is at a lower ordering temperature (energy) relative to the $x=0.3$ FM material.

C. Temperature-dependent XAS $x=0.0,0.2,0.3,0.4$

For completeness and to make contact with the work of Bridges *et al.*,[8] our results for the thermal changes in the XAS pre-edge spectra for $x\leqslant 0.4$ will be reviewed. The results for the temperature-dependent pre-edge spectra of the $x=0.0$, 0.2, 0.3, and 0.4 materials are shown in Fig. 6. (The main edge and near edge spectra are also shown in Fig. 7 for

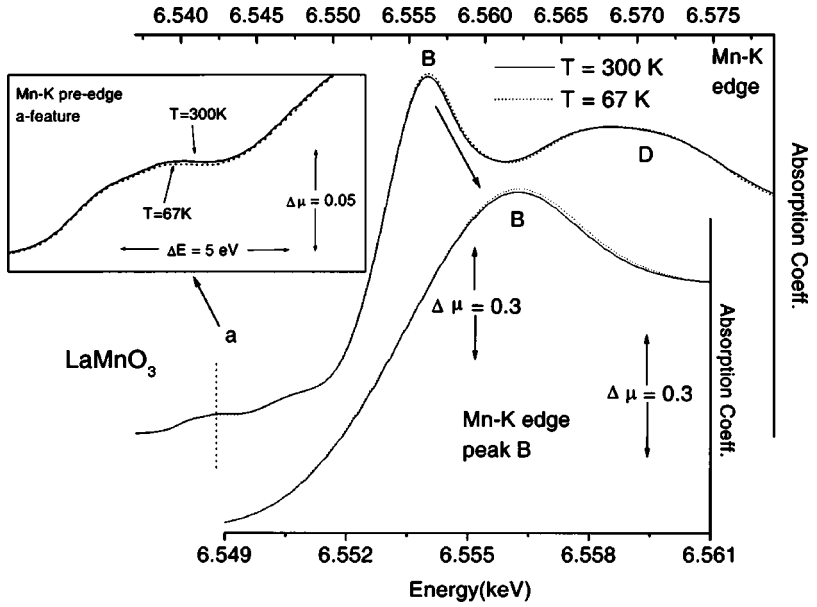

FIG. 7. The Mn *K*-edge of $LaMnO_3$ at $T=300$ and 67 K. The upper-left inset shows an expansion of the pre-edge *a*-feature region and the lower-right inset shows an expansion of the main peak *B*-feature region. While the emission spectra exhibit strong temperature dependence, the *a* features in the absorption spectra for $x=1.0$ exhibit no significant temperature dependence.

$LaMnO_3$.) These results are in accordance with those reported by Bridges *et al.*[8] in the same composition range. For the $x=0.0$ material there is very little temperature dependence of the XAS spectra including the pre-edge (as noted by Bridges *et al.*[8]). The clearest pre-edge change upon entering the low temperature, FM-metallic phase (for the $x=0.2$, 0.3, and 0.4 materials) is the enhancement/lowering-of-energy of the $a1$ feature. The low-temperature pre-edge change is maximal where the FM-ordering energy is maximal, near $x=0.3$.

Interestingly, in local-density approximation (LDA)$+U$ calculations on $LaMnO_3$ by Elfimov Anisimov, and Sawatzky[21] as well as energy bands constructed from reflectivity spectra by Jung *et al.*,[22] the $a1$ feature is associated with transitions into empty e_g majority spin states. Although much work is needed to clarify this issue, the lowering in energy of such states in the FM metal, relative to the paramagnetic (PM) insulator, is not unreasonable. Specifically, both theoretical[23,24] and experimental[25] work has emphasized the importance of: localized Jahn-Teller (JT) distortions in the PM-insulating phase at this composition; and the suppression of these localized JT distortions in the FM-metallic phase. The lowest unoccupied e_g orbital would be expected to shift down with this reduction in JT energy splitting in the paramagnetic to ferromagnetic phase change. Our pre-edge $a1$ feature results and those of Bridges *et al.*[8] are highly consistent with this scenario.

A similar thermal *d*-band shift was observed in the very early CMR material EuO.[26,27] In this system, exchange splitting of the $5d$ band accompanies the onset of the low-temperature ferromagnetic phase.

It is worth re-emphasizing that, to first order, the thermal change in these FM-metallic materials is reversed in the CO-insulating materials where the $a1$ feature was depressed. This suggest that the orbital portion of the charge/orbital ordered state may contribute a JT energy upshift of the empty e_g state at the more ''Mn^{3+}''-like sites. Such a shift would be consistent with the $a1$ feature depression in this composition range.

The disparity between the thermal XAS and XES results between the AF $x=0.0$ material[28] and the FM $x=0.3$ precludes a common explanation. Specifically: there is essentially no thermal XAS pre-edge change for the AF $x=0.0$ material but a distinct change for the FM $x=0.3$ material; whereas the thermal XES change is present, and of comparable structure/magnitude, for both the AF $x=0.0$ and FM $x=0.3$ material. Thus the argument presented above, for the XES thermal changes, is apparently not applicable to the pre-edge XAS changes. A better theoretical understanding of the XAS pre-edge is clearly motivated by this work.

V. $La_{1-x}Ca_xMnO_3$: $x=1.0$ REGIME; XES AND XAS

Figure 8 shows a comparison of Mn *K*-edge results for $CaMnO_3$ at $T=300$ and 67 K. Three regions of small but discernable spectral change can be noted for this material upon cooling. The peak *B* feature is shifted somewhat to higher energy and has its intensity somewhat enhanced. The post edge *D* feature also manifests enhanced intensity. The pre-edge feature appears to have a somewhat diminished intensity (or to ride on a smaller background from the main edge). The $a1$ pre-edge subfeature appears to have decreased intensity relative to the $a2$ subfeature. And finally, in the pre-edge region the $a3$ pre-edge subfeature is better resolved (related to the minority spin e_g band).

Clearly, the low-temperature spectral changes observed for the Mn *K*-edge of $CaMnO_3$ must be considered on a different footing from those which arose in the $x=0.5$ spectrum and which gradually diminished in the $x=0.67$ and $x=0.8$ spectra. In those materials, the competition between FM and CO energies is a plausible mechanism for the maximal effect at $x=0.5$ followed by a dying out of the effect

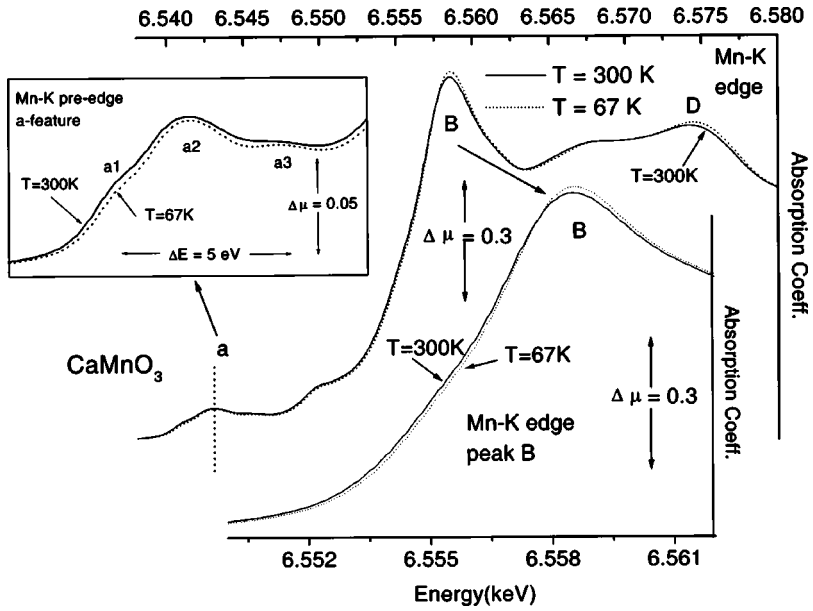

FIG. 8. The Mn *K*-edge of $CaMnO_3$ at $T=300$ and 15 K. The upper-left inset shows an expansion of the pre-edge *a*-feature region and the lower-right inset shows an expansion of the main peak *B*-feature region. In this sample, the temperature dependence of the *a*-features is quite different from all other doping values.

approaching $x=0.8$. For pure $CaMnO_3$ neither FM nor CO effects should be important.

A general sharpening of the low-temperature near-edge spectra (such as is generally known to occur in the extended x-ray-absorption fine structure region) could be one cause of these spectral changes. However, some aspects of the thermal changes in the $x=1.0$ spectrum are reminiscent of those associated with a small valence increase at low temperature. Specifically the $a1$-pre-edge feature weakening, the *B*-feature shift to higher energy, and the *D*-feature enhancement. Since covalency (and with it *d*-configuration mixing) is important in all of these manganite materials this possible explanation cannot be ignored. Indeed in both the $La_{1-x}Ca_xMnO_3$ and $Bi_{1-x}Ca_xMnO_3$ there is an extremely rapid increase in the Weiss θ parameter of the magnetic susceptibility from a small negative or positive value near $x=0.9$ to the large value of $\theta=511$ K for $x=1.0$.[29] As pointed out by Fawcett *et al.*[29] this large positive θ parameter is far out of line with the AF value of $T_N=125$ K and with the simple three dimensional *G*-type AF ordering of this material. Thus the present XAS results and previous magnetic results motivate a reconsideration of the covalency/configurational-mixing character of the end-point $CaMnO_3$ compound.

The temperature-dependent XES spectra of $CaMnO_3$ are shown in Fig. 9. The change with temperature is a broadening of the main line at low temperature with no perceptible shift in the main peak energy. Based on theoretical atomic multiplet K_β emission spectra[9] a broadening of the main lines (seen at low temperature here) can be modeled by a decrease in covalency (increase in atomic Slater integrals). Such a small formal decrease in covalency would be accompanied by a small increase in the effective charge on the Mn site and should experimentally resemble a small increase in the Mn valence. Indeed, the broadening observed is reminiscent of that seen in Fig. 1 as the Mn valence is increased, although the lack of a concomitant shift in the peak energy should be noted.

Recall that the thermal variations of the XAS manifested subtle signatures of a modest Mn-valence increase (see Fig. 3). Thus both the XES and XAS results appear consistent with a small but discernable increase in the effective Mn-site charge upon cooling $CaMnO_3$ from room to low temperature. These results reinforce the view of the Mn state in $CaMnO_3$ as a covalency/hybridization induced Mn-*d*-configuration admixture. Although the thermal energy at 300 K is small compared to the interconfiguration or hybridization energies, it is apparently not negligibly so. Hence at 300 K the configuration balance can be perturbed away from the ground-state configuration. The thermal XAS and XES effects observed are therefore related to the relaxation toward the ground-state configuration as the modest thermal perturbation is removed. Indeed, along similar lines, Fe-Mössbauer

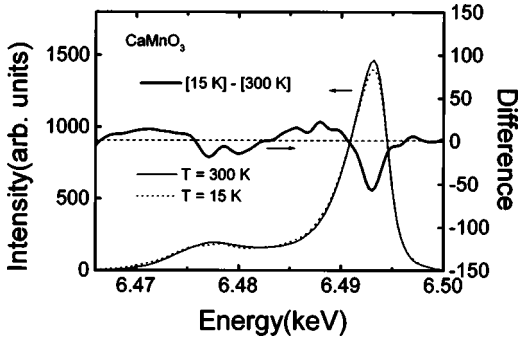

FIG. 9. A comparison of the $T=300$ K and $T=15$ K Mn K_β emission spectra of $CaMnO_3$. The difference of these two spectra is also shown with the scale for the difference spectrum (DS) appearing on the right. Note the difference in temperature response of the main line compared to that found in Figs. 2 and 5. For the Mn^{4+} state (Fig. 1), the weak satellite contribution (*s*) yields poor signal to noise ratios. Hence changes in the *s* features cannot be resolved.

experiments on related perovskite Fe compounds manifest distinct thermal variations in the isomer shift explained by thermal variations in the average Fe valence/configuration.[30]

VI. CONCLUSION

Discussions of the magnetic, transport, and phase diagram properties of the $La_{1-x}Ca_xMnO_3$ system have had substantial success starting from an ioniclike Mn^{3+}/Mn^{4+} mixture picture. While the dynamics of the hopping in these pictures can vary from fast to a slow (or even static) the Mn^{3+}/Mn^{4+} character of the bimodal local state distribution is typically not dwelt upon. Certainly all of the results and discussions of these (and related) compounds have made it clear that a fierce competition between the energies of JT, ferromagnetic, antiferromagnetic, charge state correlations interplay with the thermal energy to yield the rich phase diagram of this system.

As noted in the introduction, a number of experiments have indicated the inability of the simple Mn^{3+}/Mn^{4+} picture to account in detail for some of the properties of the $La_{1-x}Ca_xMnO_3$ system. Indeed, some of these experiments are unable to resolve the bimodal (hole vs no-hole) character of the Mn sites, suggesting instead a single (but evolving with x) Mn configuration. The importance of charge/orbital ordering in the ground states of some of these materials seems to demand inclusion of a bimodal configuration distribution. Inclusion of both perspectives involves a bimodal Mn-configuration distribution for which it is recognized from the onset that both types of sites involve covalently mixed d configurations. Within this picture the centrum and bimodality of the Mn configuration distribution are not fixed by x or the Mn^{3+}/Mn^{4+} states. Instead they can respond to the x value, the thermal energy and to the competition between the JT, ferromagnetic, antiferromagnetic, and charge state interaction energies.

At least some of the thermal variations in the XES and XAS results discussed in this paper favor a Mn configuration which is capable of responding to variations in the competing interactions and energies in the problem. It is true that the modesty of the thermal spectral changes observed here would indicate that thermal variations in the covalency factors are not dramatic. Nevertheless, their presence and their quite different character at differing x values does support the notion that covalent Mn-configuration mixing should be considered in these materials.

ACKNOWLEDGMENTS

Data acquisition was performed at Brookhaven National Laboratory's National Synchrotron Light Source which is funded by the U.S. Department of Energy. This work was supported by Department of Energy, Office of Basic Energy Sciences Grant No. DE-FG02-97ER45665. Sample preparation was supported by National Science Foundation Grant Nos. DMR-93-13106 and DMR-93-14605 (M.G.) and DMR 9802513 (S.W.C.). We thank C. H. Booth of Lawrence Berkeley National Laboratory and F. Bridges of the University of California at Santa Cruz for helpful discussions.

[1] M. F. Hundley and J. J. Neumeier, Phys. Rev. B **55**, 11 511 (1997).

[2] S. B. Oseroff, M. Torikachvili, J. Singley, S. Ali, S.-W. Cheong, and S. Schultz, Phys. Rev. B **53**, 6521 (1996).

[3] J.-H. Park, C. T. Chen, S-W. Cheong, W. Bao, G. Meigs, V. Chakarian, and Y. U. Idzerda, Phys. Rev. Lett. **76**, 4215 (1996).

[4] G. Subias, J. Garcia, M. G. Proietti, and J. Blasco, Phys. Rev. B **56**, 8183 (1997).

[5] C. H. Booth, F. Bridges, G. J. Snyder, and T. H. Geballe, Phys. Rev. B **54**, 15 606 (1996); C. H. Booth, F. Bridges, G. H. Kwei, J. M. Lawrence, A. L. Cornelius, and J. J. Neumeier, Phys. Rev. Lett. **80**, 853 (1998).

[6] M. Croft, D. Sills, M. Greenblatt, C. Lee, S.-W. Cheong, K. V. Ramanujachary, and D. Tran, Phys. Rev. B **55**, 8726 (1997).

[7] R. S. Liu, J. B. Wu, C. Y. Chang, J. G. Lin, C. Y. Huang, J. M. Chen, and R. G. Liu, J. Solid State Chem. **125**, 112 (1996); E. Pellegrin, L. H. Tjeng, F. M. F. de Groot, R. Hesper, G. A. Sawatzky, Y. Moritomo, and Y. Tokura, J. Electron Spectrosc. Relat. Phenom. **86**, 115 (1997).

[8] F. Bridges, C. H. Booth, G. H. Kwei, J. J. Neumeier, and G. A. Sawatzky, Phys. Rev. B **61**, R9239 (2000).

[9] T. A. Tyson, Q. Qian, C.-C. Kao, J.-P. Rueff, F. M. F. de Groot, M. Croft, S.-W. Cheong, M. Greenblatt, and M. A. Subramanian, Phys. Rev. B **60**, 4665 (1999).

[10] G. Peng, F. M. F. de Groot, K. Hämäläinen, J. A. Moore, X. Wang, M. M. Grush, J. B. Hastings, D. P. Siddons, W. H. Armstrong, O. C. Mullins, and S. P. Cramer, J. Am. Chem. Soc. **116**, 2914 (1994), and references therein; R. D. Cowan, *The Theory of Atomic Structure and Spectra* (University of California Press, Berkeley, 1981); K. Tsutsumi, H. Nakamori, and K. Ichikawa, Phys. Rev. B **13**, 929 (1976), and references therein; see, for example, the case of Ti in *X-Ray Spectroscopy*, edited by L. V. Azaroff (McGraw-Hill, New York, 1974), p. 507; it should be noted that the peak normalization convention used here accentuates the very low intensity satellites of the higher valence spectra where the signal is low. In fact, in view of this, the discussion of the detailed variations in weak satellites of the higher valence spectra will be deffered to further work.

[11] X. Wang, F. M. F. de Groot, and S. P. Cramer, Phys. Rev. B **56**, 4553 (1997).

[12] F. M. F. de Groot, A. Fontaine, C.-C. Kao, and M. Krisch, J. Phys.: Condens. Matter **6**, 6875 (1994).

[13] C.-C. Kao, K. Hämäläinen, M. Krisch, D. P. Siddons, T. Oversluizen, and J. B. Hastings, Rev. Sci. Instrum. **66**, 1699 (1995).

[14] P. A. Lee, P. H. Citrin, P. Eisenberger, and B. M. Kincaid, Rev. Mod. Phys. **53**, 769 (1981).

[15] K. Tsutsumi, H. Nakamori, and K. Ichikawa, Phys. Rev. B **13**, 929 (1976).

[16] Z. Zeng, M. Greenblatt, M. A. Subramanian, and M. Croft, Phys. Rev. Lett. **82**, 3164 (1999).

[17] The X19A beamline utilizes a parabolic mirror to remove the source divergence. This combined with the use of a Si (311) monochromator made possible the observation of the $a1$, $a2$, and $a3$ features in $CaMnO_3$.

[18] H. Woo *et al.* (unpublished).
[19] W. Bao, J. D. Axe, C. H. Chen, and S.-W. Cheong, Phys. Rev. Lett. **78**, 543 (1997); E. I. Turkevich and V. P. Plakhtii, Fiz. Tverd. Tela (Leningrad) **10**, 951 (1968) [Sov. Phys. Solid State **10**, 754 (1968)].
[20] A. Millis (private communications).
[21] I. S. Elfimov, V. I. Anisimov, and G. A. Sawatzky, Phys. Rev. Lett. **82**, 4264 (1999).
[22] J. H. Jung, K. H. Kim, D. J. Eom, T. W. Noh, E. J. Choi, J. Yu, Y. S. Kwon, and Y. Chung, Phys. Rev. B **55**, 15 489 (1997).
[23] A. J. Millis, Phys. Rev. B **53**, 8434 (1996).
[24] A. J. Millis, P. B. Littlewood, and B. I. Shraiman, Phys. Rev. Lett. **74**, 5144 (1995).
[25] S.-W. Cheong and H. Y. Hwang, *Colossal Magnetoresistance Oxides*, edited by Y. Tokura (Gordon & Breach, Abingdon, UK, 2000).
[26] J. Feinleib, W. J. Scouler, J. O. Dimmock, J. Hanus, T. B. Reed, and C. R. Pidgeon, Phys. Rev. Lett. **22**, 1385 (1969).
[27] H. G. Zimmer, K. Takemura, K. Syassen, and K. Fischer, Phys. Rev. B **29**, 2350 (1984).
[28] The $LaMnO_{3-\delta}$ sample and all samples used in these experiments were air annealed giving $\delta > 0$. On the other hand, Bridges *et al.* report values of ~ 0.0 of their samples.
[29] I. Fawcett, J. Sunstrom, M. Greenblatt, M. Croft, and K. Ramanujachary, Chem. Mater. **10**, 3643 (1998).
[30] P. Adler, J. Solid State Chem. **130**, 129 (1997).